BMC Musculoskeletal Disorders

RESEARCH

Open Access

Automated opportunistic screening for osteoporosis using deep learning-based automatic segmentation and radiomics on proximal femur images from low-dose abdominal CT

Changyu Du[1†], Jian He[1†], Qiye Cheng[1], Mengting Hu[1], Jingyi Zhang[1], Jiageng Shen[1], Shigeng Wang[1], Yijun Liu[1], Jianying Li[2] and Wei Wei[1*]

Abstract

Rationale and objectives To establish an automated osteoporosis detection model based on low-dose abdominal CT (LDCT). This model combined a deep learning-based automatic segmentation of the proximal femur with a radiomics-based bone status classification.

Materials and methods A total of 456 participants were retrospectively included and were divided into a development cohort comprising 355 patients, with a 7:3 ratio randomly assigned to the training and validation cohorts, and a test cohort comprising 101 patients. The automatic segmentation model for the proximal femur was trained using VB-Net. The Dice similarity coefficient (DSC) and volume difference (VD) were employed to evaluate the performance of the segmentation model. A three-classification predictive model for assessing bone mineral status was constructed utilizing radiomic analysis. The diagnostic performance of the radiomics model was assessed using the area under the curve (AUC), sensitivity, and specificity.

Results The automatic segmentation model for the proximal femur demonstrated excellent performance, achieving DSC values of 0.975 ± 0.012 and 0.955 ± 0.137 in the validation and test cohorts, respectively. In the test cohort, the radiomics model utilizing the random forest (RF) classifier achieved AUC values, sensitivity, and specificity of 0.924 (95% CI: 0.854–0.967), 0.846 (95% CI: 0.719–0.931), and 0.837 (95% CI: 0.703–0.927) for the identification of normal bone mass. For the identification of osteoporosis, the corresponding metrics were 0.960 (95% CI: 0.913-1.000), 0.947 (95% CI: 0.740–0.999), and 0.963 (95% CI: 0.897–0.992). In the case of osteopenia, the corresponding metrics were 0.828 (95% CI: 0.747–0.909), 0.767 (95% CI: 0.577–0.901), and 0.746 (95% CI: 0.629–0.842).

[†]Changyu Du and Jian He are co-first authors and have contributed equally to the work.

*Correspondence:
Wei Wei
weiweidy1988@163.com

Full list of author information is available at the end of the article

Conclusion A three-classification predictive model combining a deep learning-based automatic segmentation of the proximal femur and a radiomics-based bone status classification on LDCT images can be used for the opportunistic detection of osteoporosis.

Keywords Osteoporosis, Automatic detection, Radiomics, Deep learning, Bone mineral density, Opportunistic screening

Introduction

Osteoporosis is a systemic bone disease closely associated with population aging, characterized by decreased bone mass and deterioration of the bone microstructure, leading to increased bone fragility and a heightened risk of fractures [1, 2]. Recent studies predict that the number of major fragility fractures (wrist, vertebra and hip) in China will reach 4.83 million in 2035 and 5.99 million in 2050, with a corresponding medical expenditure of $25.43 billion [3]. Among these, hip fractures represent a significant public health burden for the elderly; approximately 20% of elderly patients with hip fractures die from various complications within one year, and about 50% of these patients become disabled [4, 5]. Given that osteoporosis is the leading cause of hip fractures [5], there is an urgent need to develop timely and effective methods for detecting hip osteoporosis.

Bone mineral density (BMD) serves as the principal measure of human bone mass and is directly associated with osteoporosis [1]. Currently, Dual-energy X-ray Absorptiometry (DXA) and Quantitative Computed Tomography (QCT) are the primary methods employed for the clinical assessment of bone density [6, 7]. However, individuals with osteoporosis often do not exhibit clear clinical symptoms until they sustain an osteoporotic fracture, leading to low detection and screening rates for the condition. Additionally, DXA employs two-dimensional imaging, which may lead to false-negative results concerning bone hyperplasia due to degenerative changes in the hip. Furthermore, the application of QCT for measuring BMD necessitates specialized software and equipment, along with stringent calibration protocols, which restricts its widespread use due to limited accessibility. Consequently, there is an urgent need to identify an efficient and straightforward method for screening proximal femoral osteoporosis.

Radiomics enhances the accuracy of disease diagnoses by extracting various medical imaging features from CT images and analyzing the quantitative information they contain [8, 9]. This field has been extensively researched in degenerative diseases, particularly osteoporosis [10–12]. Studies have demonstrated that radiomic features from hip CT images can accurately predict hip bone quality [12, 13]. Furthermore, low-dose abdominal CT (LDCT) reduces radiation exposure risks for patients, making it a common choice for health check-ups and follow-ups for various conditions, while at the same time, these images provide valuable information about proximal femur bone density. The integration of LDCT with bone density assessments is a cost-effective approach that does not impose additional radiation exposure or financial burdens on patients. On the other hand, prior studies on proximal femur segmentation primarily relied on manual methods performed by radiologists, contributing to an increased workload [12, 14]. Recent research indicates that deep learning-based automatic segmentation of the proximal femur can substantially alleviate the manual workload of radiologists, thereby enhancing workflow efficiency [15]. However, to our knowledge, few studies have applied automatic segmentation models based on LDCT and radiomics-based classification models of bone quality for the opportunistic screening of osteoporosis.

The purpose of our study is twofold. First, to develop a deep learning-based automatic segmentation model for the proximal femur using LDCT images, and to evaluate its accuracy in segmenting the proximal femur. Second, to create a radiomic model based on this automatic segmentation to assess bone status across three categories, aiming to provide automatic and accurate opportunistic detection for osteoporosis.

Materials and methods

Patient enrollment

The study was conducted in accordance with the Declaration of Helsinki (as revised in 2013). The study was approved by the ethics committee/IRB of The First Affiliated Hospital of Dalian Medical University (no. PJ-KS-KY-2023-276) and individual informed consent to participate for this retrospective analysis was waived by the ethics committee/IRB of The First Affiliated Hospital of Dalian Medical University.

We retrospectively screened 695 patients who underwent LDCT and QCT examinations within one week from January 2024 to November 2024. The exclusion criteria were as follows: [1] patients with bone metastases ($n=40$) [2], metastasis outside the bone ($n=58$) [3], hip fracture ($n=42$) [4], hip replacement ($n=49$), and [5] incomplete CT scans ($n=50$). Finally, a total of 456 patients were included in our study. These patients were divided into a development cohort consisting of 355 patients, who were randomly assigned to the training and validation cohorts in a 7:3 ratio, and a test cohort comprising 101 patients, based on the time of examination. The patient selection process is illustrated in Fig. 1. The

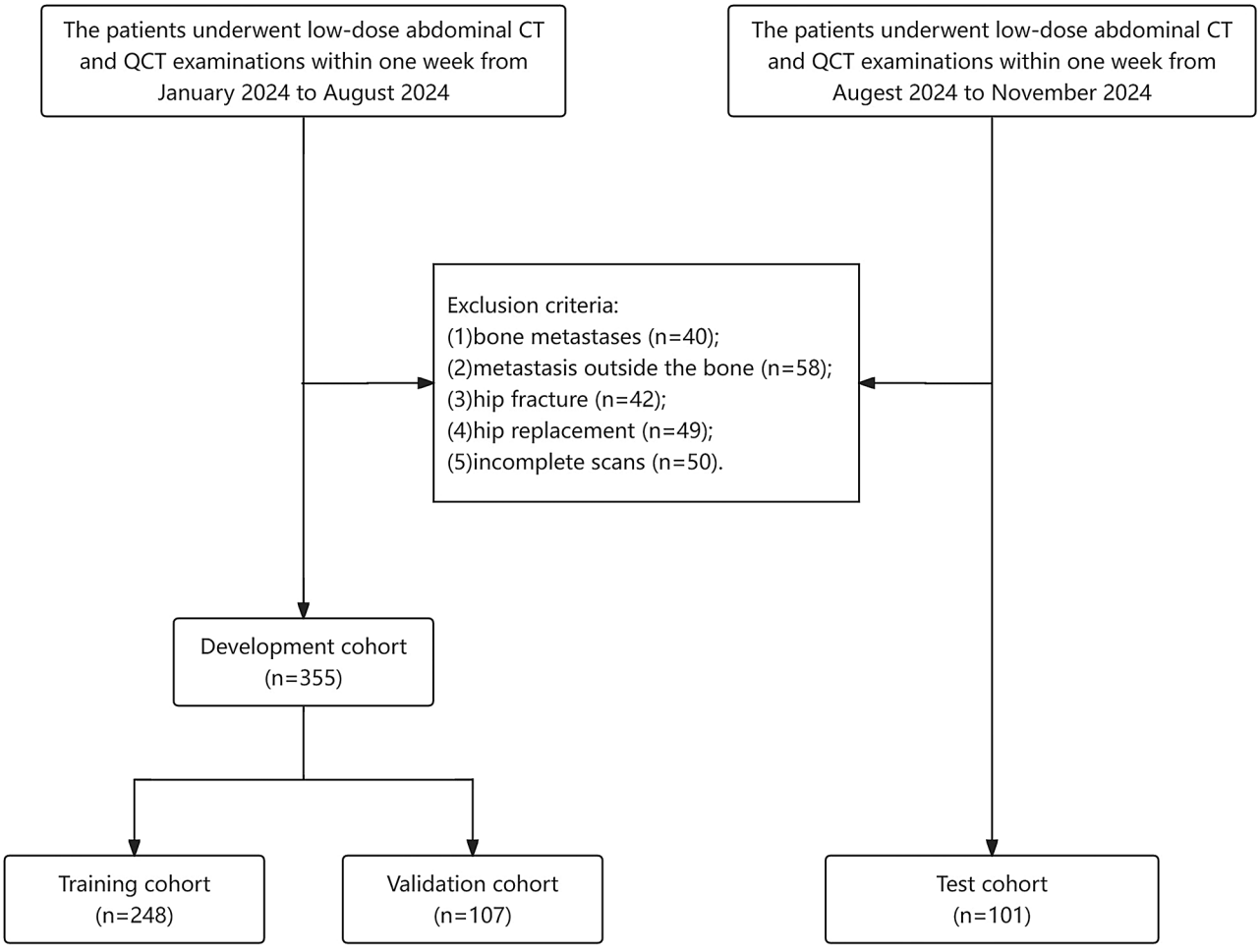

Fig. 1 Flowchart for the study design and patient selection. QCT, quantitative computed tomography

construction of the auto-segmentation framework, along with the extraction of radiomics features, feature selection, and the development and evaluation of machine learning models, was conducted using the uAI Research Portal V1.1 (Shanghai United Imaging Intelligence, Co., Ltd.), as illustrated in Fig. 2.

CT images

LDCT examinations were conducted using a 256-row CT scanner (Revolution CT, GE HealthCare, Milwaukee, WI, USA). The scanning range for all patients extended from the roof of the diaphragm to 3.5 cm below the lesser trochanter, encompassing the entire hip joint. The imaging parameters employed were as follows: tube voltage of 120 kVp, automatic tube current, (50–400 mA) with noise index set as 14, (which requires approximately 62% of the radiation dose for the routine abdominal CT with a noise index of 11), tube rotation speed of 0.5 s/r, detector width of 80 mm, and pitch of 0.992. All raw data were reconstructed using a standard kernel, incorporating 60% adaptive statistical iterative reconstruction-Veo (ASIR-V), with a slice thickness and interval of 1.25 mm.

QCT acquisition

All bone density measurements were carried out on a specialized QCT Pro workstation (version 6.1, Mindways Software, Inc.) using the reconstructed LDCT images. Quality control analyses were conducted weekly using the asynchronous calibration phantom (Model 4, Mindways Software, Inc.). The system automatically identifies the region of interest (ROI) in the femoral neck and the entire hip, subsequently calculating the BMD and T-scores for the femoral neck, trochanter, intertrochanter, and the entire hip. According to the diagnostic criteria established by the International Society for Clinical Densitometry (ISCD) and the American College of Radiology (ACR) [16], osteoporosis is defined as a T-score ≤ -2.5, osteopenia as a T-score < -1 and > -2.5, and normal BMD as a T-score ≥ -1. The patients were classified into three groups: osteoporosis, osteopenia, and normal bone density.

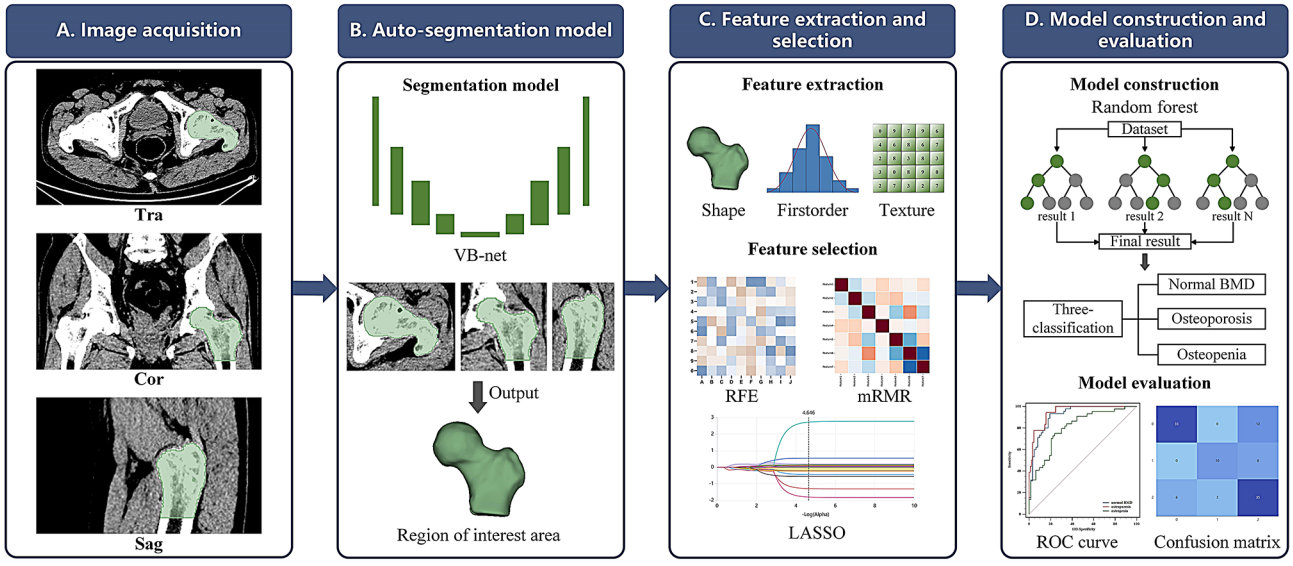

Fig. 2 Workflow of this study. RFE, recursive feature elimination; mRMR, minimum-redundancy maximum-relevancy; LASSO, least absolute shrinkage and selection operator

Image segmentation

To evaluate the reproducibility of manual segmentation between observers, we randomly selected 100 patients from the training cohort. Two readers, J. He and Y. Liu, with 3 and 15 years of experience in musculoskeletal radiology, respectively, manually outlined the volumes of interest (VOIs) of the proximal femur, extending from the femoral head to the level of the lower trochanter, situated above the horizontal line marking the lower margin of the ischial tuberosity. The delineation encompassed the entire medullary cavity and cortical bone while carefully excluding regions of hyperplastic bone. The Dice similarity coefficient (DSC) was employed to assess the inter-observer segmentation consistency. If a satisfactory agreement was reached, the junior radiologist proceeded to complete the remaining cases under the supervision of the senior radiologist.

We employed the VB-Net network framework to conduct automatic segmentation of the proximal femur. The segmentation module in the uAI Research Portal (uRP) is capable of automatically delineating ROI from both single-modal and multimodal 2D and 3D data. The VB-Net architecture is one of the partitioning architectures implemented for this purpose. The network structure is presented in Supplementary Fig. 1. Our proximal femur segmentation model consists of two concatenated VB-Nets. Initially, global sampling is applied in the coarse segmentation as model 1, where the image is resampled to dimensions of $3 \times 3 \times 3$ mm using B-spline interpolation. Subsequently, in the fine segmentation as model 2, the image is resampled to yield a high-resolution local image with voxel dimensions of $1 \times 1 \times 1$ mm, sampled through a mask. The parameters are set as follows: learning rate of 1×10^{-4}, batch size of 8, epochs of 1001, and using Adam optimizer. The focal loss function is utilized to monitor the convergence of the training model and to optimize the network. DSC and volume difference (VD, defined as the manually delineated volume minus the automatically segmented volume) were employed to evaluate the performance of the segmentation model.

Radiomics feature extraction

All images were normalized using gray discretization with a bin width of 25, and the voxel spacing was resampled to $1 \times 1 \times 1$ mm utilizing the B-spline interpolation method. Subsequently, radiomic features were extracted from each ROI, including both original features and higher-order features processed using wavelet and Laplacian of Gaussian (LoG) filters. Ultimately, a total of 1,184 two-dimensional (2D) and three-dimensional (3D) features were extracted from the original images. These features were classified into several categories: first-order features, shape features, gray level co-occurrence matrix (GLCM) features, gray level size zone matrix (GLSZM) features, gray level run length matrix (GLRLM) features, gray level distance matrix (GLDM) features, and neighborhood gray tone difference matrix (NGTDM) features.

Features selection and model construction

Recursive Feature Elimination (RFE), Maximum Relevance and Minimum Redundancy (mRMR), and the Least Absolute Shrinkage and Selection Operator (LASSO) were employed for stepwise feature selection. RFE effectively reduces the dimensionality of image omics parameters, addressing the issues of overfitting and enhancing classification accuracy. mRMR minimizes redundancy

Table 1 Characteristics of patients in the training, validation and test cohorts

Characteristic	Training cohort	Validation cohort	Test cohort	*P* value
Age(years) [a]	67.17 ± 8.52	66.57 ± 8.42	67.65 ± 6.33	0.623
Gender(n)				0.516
Male	121(48.79%)	53(49.53%)	43(42.57%)	
Female	127(51.21%)	54(50.47%)	58(57.43%)	
Classification(n)				0.376
Normal	105(42.34%)	45(42.06%)	52(51.49%)	
Osteopenia	101(40.73%)	44(41.12%)	30(29.70%)	
Osteoporosis	42(16.93%)	18(16.82%)	19(18.81%)	

[a] Data are expressed as mean ± standard deviation

Table 2 Detailed results of automatic segmentation accuracy in all cohorts

Cohort	Group	Dice [a]	VD (cm^3) [b]
Validation cohort	All patients	0.975 ± 0.012	0.057(0.022,0.129)
	Normal	0.979 ± 0.009	0.058(0.022,0.132)
	Osteopenia	0.973 ± 0.012	0.058(0.022,0.142)
	Osteoporosis	0.966 ± 0.017	0.058(0.023,0.132)
Test cohort	All patients	0.955 ± 0.137	0.041(0.021,0.068)
	Normal	0.956 ± 0.135	0.042(0.021,0.068)
	Osteopenia	0.944 ± 0.178	0.041(0.021,0.068)
	Osteoporosis	0.967 ± 0.011	0.047(0.023,0.068)

[a] Data are expressed as mean ± standard deviation

[b] Data are expressed as medians (25-75th percentile)

VD volume difference

among features while preserving the most relevant attributes related to bone density. Subsequently, LASSO was utilized to select the optimal radiomics features. A three-category classification model was developed using a random forest (RF) classifier to simultaneously differentiate among normal bone mass, osteoporosis, and osteopenia. Receiver operating characteristic (ROC) curves were constructed, and the area under the curve (AUC), along with sensitivity, specificity, and accuracy, was calculated to evaluate the performance of the model.

Statistical analysis

All data were statistically analyzed using SPSS version 24.0 (SPSS Inc., Chicago, IL, USA), R package (version 4.2.1) and Medcalc version 20.2 (Medcalc, Ltd, Ostend, Belgium), with the Kolmogorov-Smirnov test employed to assess data normality. Quantitative data that followed a normal distribution are reported as mean ± standard deviation (SD), while those that did not meet this criterion are presented as medians (25-75th percentile). One-way ANOVA was conducted to compare age and radiation dose distributions across the training, validation, and test cohort, whereas Chi-square tests evaluated gender differences. The effectiveness of radiomics in classifying bone status was assessed through ROC curves. The AUC, sensitivity, specificity, and accuracy were derived from the ROC analysis, and the 95% confidence intervals for these metrics were calculated using the Wilson Score method. A *P*-value of less than 0.05 was deemed statistically significant.

Results

Patient baseline information

A total of 456 patients (217 males and 239 females, mean age, 67.80 ± 8.18; range, 50–91 years) were included in this study. Among the participants, 202 were diagnosed with normal bone mass, 175 with osteopenia, and 79 with osteoporosis based on the QCT T-score. There were no statistically significant differences in the baseline information among the training, validation, and test cohorts. Table 1 presents the demographic characteristics of study participants in these three cohorts. The average radiation dose administered to all patients was 241.30 mGy·cm and 3.62 mSv; detailed information regarding the radiation doses is available in the supplementary Table S1.

Automatic segmentation model

The segmentation of the proximal femur revealed a high degree of consistency between the two reviewers, with a mean DSC of 0.989 ± 0.002. The automatic segmentation model for the proximal femur exhibited excellent performance, achieving DSC values of 0.975 ± 0.012 and 0.955 ± 0.137 in the validation and test cohorts, respectively. The VD did not exceed 1 cm^3, with mean values of 0.057 (0.022, 0.129) and 0.041 (0.021, 0.068) in the validation and test cohorts, respectively. Detailed segmentation results are presented in Table 2.

Radiomics model

A total of 1184 radiomic features were extracted from the VOIs on LDCT images. RFE selected 50 features from this initial set. Then 20 features were selected using the mRMR method. Ultimately, 15 optimized features were selected through LASSO regression and used to establish the RF model. The specific features and their correlation coefficients are presented in Fig. 3.

In the test cohort, the radiomics model utilizing the RF classifier achieved AUC values, sensitivity, specificity, and accuracy of 0.924 (95% CI: 0.854–0.967), 0.846, 0.837, and 0.842 for the identification of normal bone mass. For the identification of osteoporosis, the corresponding metrics were 0.960 (95% CI: 0.901–0.989), 0.947, 0.963, and 0.960. In the case of osteopenia, the corresponding metrics were 0.828 (95% CI: 0.740–0.896), 0.767, 0.746, and 0.752. Detailed performance metrics are presented in Table 3, while Fig. 4 displays the confusion matrix for the model. The ROC curves are presented in Fig. 5.

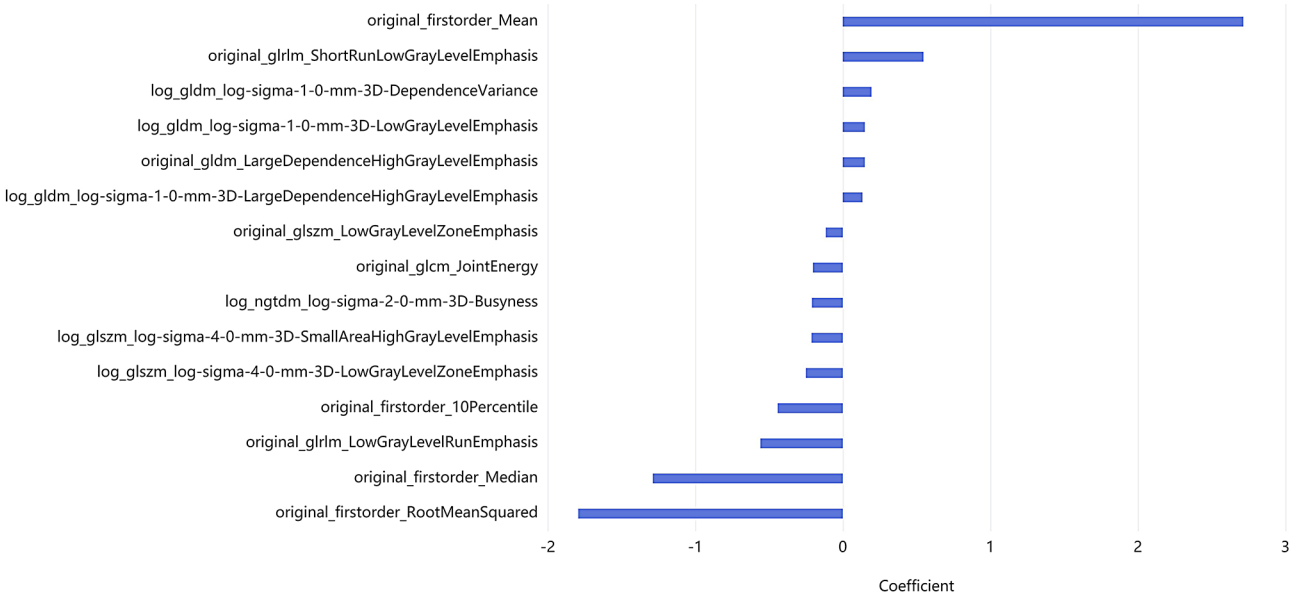

Fig. 3 Image features and correlation coefficient

Table 3 Diagnostic efficiency of the radiomics model in the training, validation and test cohorts

Cohort	Category	AUC	95% CI	Sensitivity	95% CI	Specificity	95% CI	Accuracy	95% CI
Training	Normal	0.936	0.906-0.965	0.865	0.784-0.924	0.888	0.825-0.935	0.879	0.831-0.917
	Osteopenia	0.913	0.877-0.949	0.743	0.646-0.824	0.939	0.887-0.972	0.859	0.809-0.900
	Osteoporosis	0.961	0.922-1.000	0.905	0.774-0.973	0.961	0.925-0.983	0.951	0.917-0.975
Validation	Normal	0.920	0.870-0.970	0.933	0.817-0.986	0.806	0.686-0.896	0.860	0.779-0.919
	Osteopenia	0.806	0.722-0.889	0.750	0.597-0.868	0.762	0.638-0.860	0.757	0.665-0.835
	Osteoporosis	0.948	0.906-0.990	0.944	0.727-0.999	0.843	0.750-0.911	0.860	0.779-0.919
Test	Normal	0.924	0.877-0.971	0.846	0.719-0.931	0.837	0.703-0.927	0.842	0.756-0.907
	Osteopenia	0.828	0.747-0.909	0.767	0.577-0.901	0.746	0.629-0.842	0.752	0.657-0.833
	Osteoporosis	0.960	0.913-1.000	0.947	0.740-0.999	0.963	0.897-0.992	0.960	0.902-0.989

CI: confidence interval

Discussion

In this study, we developed a deep learning-based automated segmentation model for the proximal femur and a radiomics-based bone status classification model for osteoporosis screening utilizing LDCT images. The results demonstrated that the automatic segmentation model for the proximal femur exhibited strong discriminative efficiency, with the mean DSC of 0.975 ± 0.012 and 0.955 ± 0.137 in the validation and test cohorts, respectively. Furthermore, the radiomics model demonstrated excellent prediction performance for normal bone density, osteoporosis, and osteopenia with the AUC of 0.924, 0.960, 0.828 in the test cohort.

Currently, DXA and QCT are the primary modalities for clinically measuring bone mineral density and diagnosing osteoporosis. DXA utilizes two-dimensional imaging, which may result in false-negative outcomes related to bone hyperplasia due to degenerative changes in the patient's hip [17, 18]. In contrast, the QCT measurements of bone density are unaffected by degenerative changes or surrounding soft tissues, and its accuracy has been extensively validated in clinical studies [19, 20]. Nevertheless, the application of QCT for measuring bone mineral density necessitates specialized software and equipment, along with rigorous calibration. These factors collectively hinder the early screening of osteoporosis. In recent years, opportunistic osteoporosis screening has been gaining momentum [21], as a single CT scan can provide additional bone mineral density information while facilitating the diagnosis of the disease, thereby achieving comprehensive osteoporosis screening. In clinical practice, abdominal CT scans are efficient and rapid, serving as a fundamental method for examining abdominal diseases. These scans not only facilitate the diagnosis of such diseases but also provide information on bone density in the hip region. Moreover, radiomics enables the extraction of a vast number of features from CT images in a high-throughput manner, allowing for deeper analysis that assists physicians in making more precise diagnoses. Yuan et al. [14] discovered that a

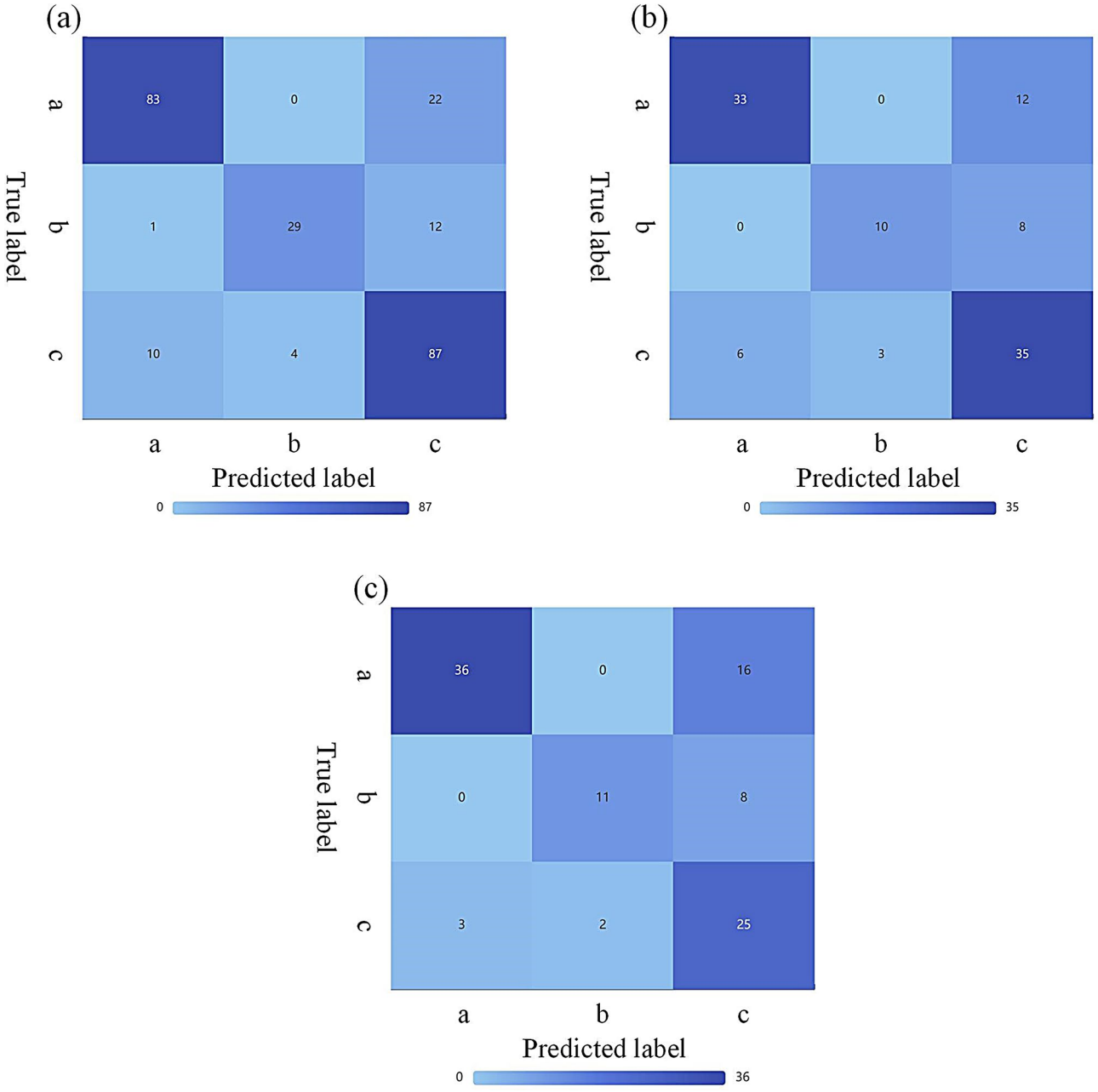

Fig. 4 The confusion matrix for the model in the (**a**) training (**b**) validation, and (**c**) test cohorts. **a**. normal BMD; **b**. osteoporosis; **c**. osteopenia

radiomic model based on the proximal femur could identify abnormalities in bone quantity. Fang et al. [12] combined radiomic models with clinical features to develop a nomogram predictive model for osteoporosis. Lim et al. [22] reported that the RF model based on abdomen-pelvic CT exhibited high predictive performance for identifying osteoporosis, with AUC values of 0.959 in the training cohort and 0.960 in the testing cohort. However, these studies have predominantly focused on conventional abdominal CT images for osteoporosis prediction. With growing health awareness, low-dose CT scan technology has gained significant attention. Studies have demonstrated that low-dose scanning reduces radiation exposure while maintaining comparable diagnostic capability to conventional CT [23]. Thus, establishing radiomic models on LDCT images for opportunistic osteoporosis screening is significant. Furthermore, the studies mentioned previously all utilized manual segmentation of the proximal femur, which undoubtedly adds to the workload of radiologists.

Deep learning-based convolutional neural networks (CNNs) exhibit strong performance in segmenting vertebral bodies and pelvic regions [24–26]. This method facilitates osteoporosis screening in large demographic

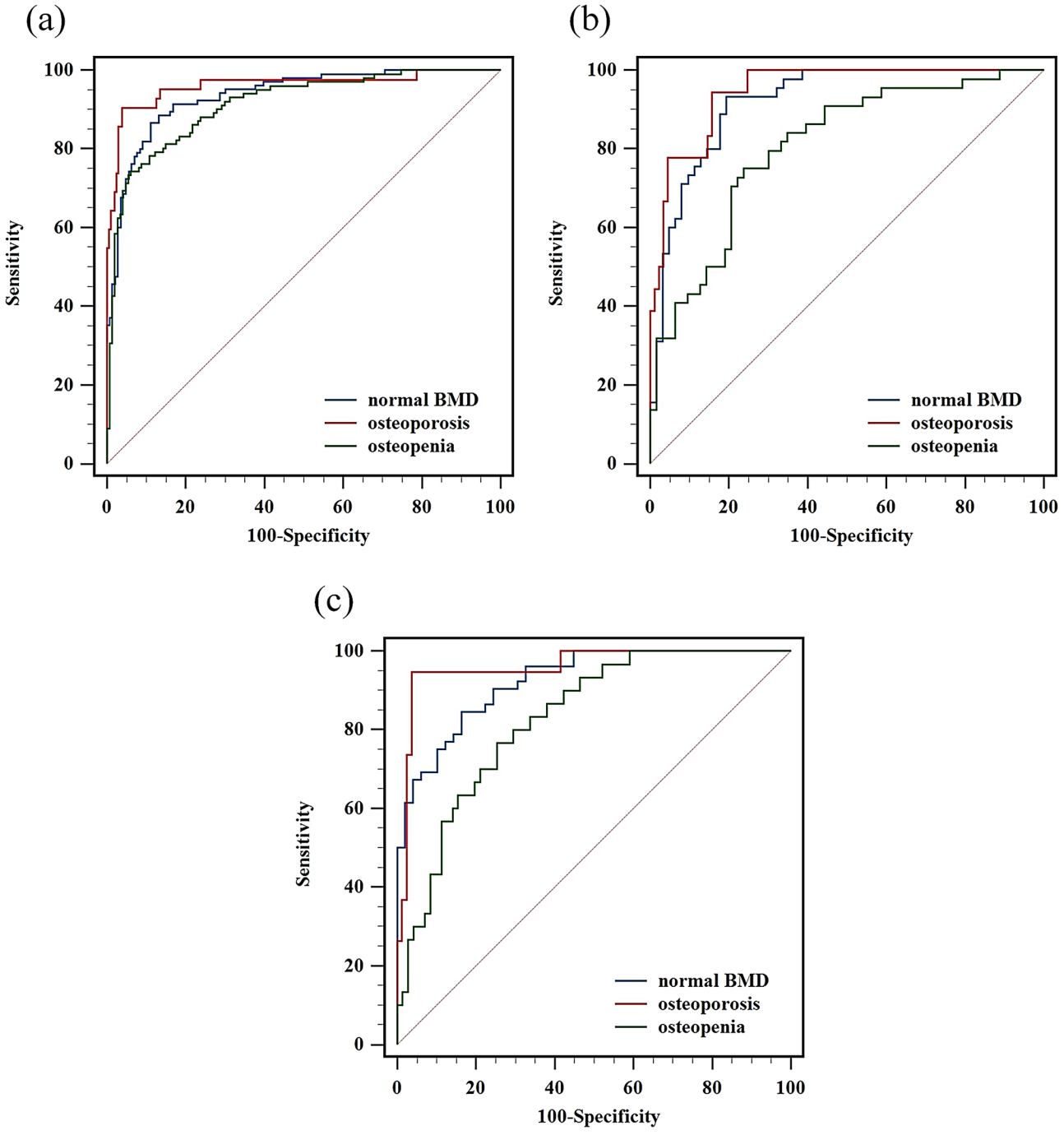

Fig. 5 The ROC curves for the prediction of BMD in the (**a**) training (**b**) validation, and (**c**) test cohorts. ROC, receiver operating characteristic; BMD, bone mineral density

populations. In our study, we developed an automatic segmentation model for the proximal femur based on VB-Net. VB-Net is an enhanced version of several classic CNN architectures that employs a bottleneck structure in place of the traditional convolutional layers found in V-Net (with "B" representing bottleneck), thereby reducing the number of parameters and accelerating the network's convergence speed [27, 28]. VB-Net has been widely applied in clinical practice [28–30]. Pan et al. [29] employed VB-Net for the automatic segmentation of trigeminal neuralgia, achieving an average Dice Similarity Coefficient (DSC) of 0.74 ± 0.08 in the testing set. Similarly, Wang et al. [31] demonstrated strong performance in the automatic segmentation of thoracic vertebrae, with average DSC values surpassing 0.93. In our study, the VB-Net-based automatic segmentation model for

the proximal femur displayed exceptional discriminative performance, with DSC values exceeding 0.94 in both the testing cohort and the test cohort. Moreover, the volume difference remained below 1 cm^3, aligning with the findings of prior studies.

Our study successfully implemented automatic segmentation to replace manual segmentation in LDCT scans, leading to the establishment of a three-classification model that simultaneously differentiates among normal bone density, osteoporosis, and osteopenia. We used RF classifier to develop the radiomics model. The RF classifier comprises a collection of decision trees constructed on random subsets of the input space. Each decision tree is built from a bootstrap sample dataset, which randomly selects features for splits, ultimately classifying and integrating predictions to enhance accuracy and generalization [32]. The RF classifier demonstrates strong performance in assessing bone density [31, 33]. In our study, the RF classifier was equally effective in distinguishing among the three bone density states. The AUC values for distinguishing normal bone density, osteoporosis, and bone mass reduction were 0.920, 0.948, and 0.806, respectively, in the validation cohort, and 0.924, 0.960, and 0.828, respectively, in the test cohort. However, when distinguishing osteopenia, the AUC value slightly decreased, because unlike the single thresholds for normal bone density (BMD T-value > -1) and osteoporosis (BMD T-value < -2.5), the diagnosis of bone mass reduction requires meeting both conditions of T-value greater than −2.5 and less than −1 simultaneously. This dual threshold complicates model learning and increases the likelihood of classification errors. Nonetheless, in our study, the AUC value for distinguishing osteopenia remained above 0.80 in the test cohorts, indicating a high level of efficacy.

However, this study presents certain limitations. Firstly, this was a single-center investigation, with all CT scans conducted on the same CT machine. Further multicenter, large-sample external validation is required to support the model's robustness. Additionally, this study exclusively extracted radiomics features from the proximal femur. Future research will integrate clinical data to develop a combined model that further enhances diagnostic efficacy and validates the model's generalizability. Furthermore, our study has not yet developed a model based on diagnostic physicians or an AI-assisted model for their benefit. Future research will investigate the efficacy of radiomics models in supporting physician decision-making in diagnosis.

In conclusion, our research findings provide preliminary evidence that combining deep learning automatic segmentation models with radiomics models can facilitate opportunistic screening for osteoporosis of the proximal femur in LDCT scans.

Abbreviations

ASIR-V	adaptive statistical iterative reconstruction-Veo
AUC	area under the curve
CT	computed tomography
LDCT	low-dose abdominal CT
ROC	receiver operating characteristic
ROI	region of interest
VOI	volume of interest
DSC	dice similarity coefficient
VD	volume difference
RF	random forest
BMD	bone mineral density
DXA	dual-energy X-ray Absorptiometry
QCT	quantitative computed tomography
ISCD	international society for clinical densitometry
ACR	American college of radiology
uRP	uAI Research Portal
LoG	Laplacian of Gaussian
GLCM	gray level co-occurrence matrix
GLSZM	gray level size zone matrix
GLRLM	gray level run length matrix
GLDM	gray level distance matrix
NGTDM	neighborhood gray tone difference matrix
RFE	recursive feature elimination
mRMR	maximum relevance and minimum redundancy
LASSO	least absolute shrinkage and selection operator
CNNs	convolutional neural networks

Supplementary Information

The online version contains supplementary material available at https://doi.org/10.1186/s12891-025-08631-x.

Supplementary Material 1

Acknowledgements
Not applicable.

Author contributions
All authors have significantly contributed to the analysis and interpretation of the data, manuscript drafting, and critical intellectual content revision, and have given their final approval for the submitted version. Changyu Du and Jian He: Conception, design and writing original draft. Qiye Cheng and Mengting Hu: Provision of study materials or patients. Changyu Du and Jingyi Zhang: Design, collection of data and review. Jiageng Shen and Shigeng Wang: Data analysis and Data curation. Yijun Liu and Wei Wei: Supervision and administrative support. Jianying Li: formal analysis and editing.

Funding
This research did not receive any specific grant from funding agencies in the public, commercial, or not-for-profit sectors.

Data availability
The datasets in this study are available on request from the corresponding author. The datasets are not publicly available due to privacy or ethical restrictions.

Declarations

Ethics approval and consent to participate
The study was conducted in accordance with the Declaration of Helsinki (as revised in 2013). The study was approved by the ethics committee/IRB of The First Affiliated Hospital of Dalian Medical University (no. PJ-KS-KY-2023-276) and individual informed consent to participate for this retrospective analysis was waived by the ethics committee/IRB of The First Affiliated Hospital of Dalian Medical University.

Consent for publication
Not applicable.

Competing interests
The authors declare no competing interests.

Author details
[1]Department of Radiology, First Affiliated Hospital of Dalian Medical University, Xigang District, Lianhe Road, No.193, Dalian, China
[2]CT Research, GE Healthcare, Dalian, China

Received: 21 January 2025 / Accepted: 8 April 2025
Published online: 17 April 2025

References

1. Noh JY, Yang Y, Jung H. Molecular Mechanisms and Emerging Therapeutics for Osteoporosis. Int J Mol Sci. 2020;21(20):7623. Published 2020 Oct 15. https://doi.org/10.3390/ijms21207623
2. Gruenewald LD, Koch V, Yel I, et al. Association of Phantomless Dual-Energy CT-based volumetric bone mineral density with the prevalence of acute insufficiency fractures of the spine. Acad Radiol. 2023;30(10):2110–7. https://doi.org/10.1016/j.acra.2022.11.020.
3. Si L, Winzenberg TM, Jiang Q, Chen M, Palmer AJ. Projection of osteoporosis-related fractures and costs in China: 2010–2050. Osteoporos Int. 2015;26(7):1929–37. https://doi.org/10.1007/s00198-015-3093-2.
4. Osnes EK, Lofthus CM, Meyer HE, et al. Consequences of hip fracture on activities of daily life and residential needs. Osteoporos Int. 2004;15(7):567–74. https://doi.org/10.1007/s00198-003-1583-0.
5. Wang O, Hu Y, Gong S, et al. A survey of outcomes and management of patients post fragility fractures in China. Osteoporos Int. 2015;26(11):2631–40. https://doi.org/10.1007/s00198-015-3162-6.
6. Berry ME. Using DXA to identify and treat osteoporosis in pediatric patients. Radiol Technol. 2018;89(3):312–7.
7. Wu Y, Guo Z, Fu X, et al. The study protocol for the China health big data (China Biobank) project. Quant Imaging Med Surg. 2019;9(6):1095–102. https://doi.org/10.21037/qims.2019.06.16.
8. Aerts HJ, Velazquez ER, Leijenaar RT et al. Decoding tumour phenotype by noninvasive imaging using a quantitative radiomics approach [published correction appears in Nat Commun. 2014;5:4644. Cavalho, Sara [corrected to Carvalho, Sara]]. Nat Commun. 2014;5:4006. Published 2014 Jun 3. https://doi.org/10.1038/ncomms5006
9. Davnall F, Yip CS, Ljungqvist G, et al. Assessment of tumor heterogeneity: an emerging imaging tool for clinical practice? Insights Imaging. 2012;3(6):573–89. https://doi.org/10.1007/s13244-012-0196-6.
10. Rastegar S, Vaziri M, Qasempour Y, et al. Radiomics for classification of bone mineral loss: A machine learning study. Diagn Interv Imaging. 2020;101(9):599–610. https://doi.org/10.1016/j.diii.2020.01.008.
11. Xie Q, Chen Y, Hu Y et al. Development and validation of a machine learning-derived radiomics model for diagnosis of osteoporosis and osteopenia using quantitative computed tomography. BMC Med Imaging. 2022;22(1):140. Published 2022 Aug 8. https://doi.org/10.1186/s12880-022-00868-5
12. Fang K, Zheng X, Lin X, Dai Z. Unveiling osteoporosis through radiomics analysis of hip CT imaging. Acad radiol. Published Online Oct. 2023;27. https://doi.org/10.1016/j.acra.2023.10.009.
13. Lim HK, Ha HI, Park SY, Han J. Prediction of femoral osteoporosis using machine-learning analysis with radiomics features and abdomen-pelvic CT: A retrospective single center preliminary study. PLoS ONE. 2021;16(3):e0247330. https://doi.org/10.1371/journal.pone.0247330. Published 2021 Mar 4.
14. Yuan X, Liang Y, Yang H, et al. Applying machine learning analysis based on proximal femur of abdominal computed tomography to screen for abnormal bone mass in femur. Acad Radiol. 2024;31(5):2003–10. https://doi.org/10.1016/j.acra.2023.10.035.
15. Park MS, Ha HI, Lim HK, Han J, Pak S. Femoral osteoporosis prediction model using autosegmentation and machine learning analysis with pyradiomics on abdomen-pelvic computed tomography (CT). Quant Imaging Med Surg. 2024;14(6):3959–69. https://doi.org/10.21037/qims-23-1751.
16. American College of Radiology. (2021) ACR–SPR–SSR practice parameter for the performance of musculoskeletal quantitative computed tomography (QCT). Available at: https://www.acr.org/-/media/ACR/Files/Practice-Parameters/qct.pdf? la = en. Accessed February 23, 2021.
17. Dimai HP. Use of dual-energy X-ray absorptiometry (DXA) for diagnosis and fracture risk assessment; WHO-criteria, T- and Z-score, and reference databases. Bone. 2017;104:39–43. https://doi.org/10.1016/j.bone.2016.12.016.
18. Bolotin HH. DXA in vivo BMD methodology: an erroneous and misleading research and clinical gauge of bone mineral status, bone fragility, and bone remodelling. Bone. 2007;41(1):138–54. https://doi.org/10.1016/j.bone.2007.02.022.
19. Engelke K, Lang T, Khosla S, et al. Clinical use of quantitative computed tomography (QCT) of the hip in the management of osteoporosis in adults: the 2015 ISCD official Positions-Part I. J Clin Densitom. 2015;18(3):338–58. https://doi.org/10.1016/j.jocd.2015.06.012.
20. Löffler MT, Jacob A, Valentinitsch A, et al. Improved prediction of incident vertebral fractures using opportunistic QCT compared to DXA. Eur Radiol. 2019;29(9):4980–9. https://doi.org/10.1007/s00330-019-06018-w.
21. Jang S, Graffy PM, Ziemlewicz TJ, Lee SJ, Summers RM, Pickhardt PJ. Opportunistic osteoporosis screening at routine abdominal and thoracic CT: normative L1 trabecular Attenuation values in more than 20 000 adults. Radiology. 2019;291(2):360–7. https://doi.org/10.1148/radiol.2019181648.
22. Lim HK, Ha HI, Park SY, Han J. Prediction of femoral osteoporosis using machine-learning analysis with radiomics features and abdomen-pelvic CT: A retrospective single center preliminary study. PLoS ONE. 2021;16(3):e0247330. https://doi.org/10.1371/journal.pone.0247330. Published 2021 Mar 4.
23. Stigbrand H, Brown K, Olivecrona H, Ullmark G. Implant migration and bone mineral density measured simultaneously by low-dose CT scans: a 2-year study on 17 acetabular revisions with impaction bone grafting. Acta Orthop. 2020;91(5):571–5. https://doi.org/10.1080/17453674.2020.1769295.
24. Chen YC, Li YT, Kuo PC, et al. Automatic segmentation and radiomic texture analysis for osteoporosis screening using chest low-dose computed tomography. Eur Radiol. 2023;33(7):5097–106. https://doi.org/10.1007/s00330-023-09421-6.
25. Beckmann NM. The rising utilization of opportunistic CT screening and machine learning in bone mineral density. Can Assoc Radiol J. 2023;74(4):616–7. https://doi.org/10.1177/08465371231176716.
26. Pan Y, Shi D, Wang H, et al. Automatic opportunistic osteoporosis screening using low-dose chest computed tomography scans obtained for lung cancer screening. Eur Radiol. 2020;30(7):4107–16. https://doi.org/10.1007/s00330-020-06679-y.
27. Shi F, Hu W, Wu J, et al. Deep learning empowered volume delineation of whole-body organs-at-risk for accelerated radiotherapy. Nat Commun. 2022;13(1):6566. https://doi.org/10.1038/s41467-022-34257-x. Published 2022 Nov 2.
28. Peng T, Zeng X, Li Y, et al. A study on whether deep learning models based on CT images for bone density classification and prediction can be used for opportunistic osteoporosis screening. Osteoporos Int. 2024;35(1):117–28. https://doi.org/10.1007/s00198-023-06900-w.
29. Pan L, Wang X, Ge X et al. Application research on the diagnosis of classic trigeminal neuralgia based on VB-Net technology and radiomics. BMC Med Imaging. 2024;24(1):246. Published 2024 Sep 16. https://doi.org/10.1186/s12880-024-01424-z
30. Ma CY, Zhou JY, Xu XT, et al. Deep learning-based auto-segmentation of clinical target volumes for radiotherapy treatment of cervical cancer. J Appl Clin Med Phys. 2022;23(2):e13470. https://doi.org/10.1002/acm2.13470.
31. Wang S, Tong X, Fan Y, et al. Combining deep learning and radiomics for automated, objective, comprehensive bone mineral density assessment from Low-Dose chest computed tomography. Acad Radiol. 2024;31(3):1180–8. https://doi.org/10.1016/j.acra.2023.08.030.
32. Valentinitsch A, Trebeschi S, Kaesmacher J, et al. Opportunistic osteoporosis screening in multi-detector CT images via local classification of textures. Osteoporos Int. 2019;30(6):1275–85. https://doi.org/10.1007/s00198-019-04910-1.
33. Xue Z, Huo J, Sun X et al. Using radiomic features of lumbar spine CT images to differentiate osteoporosis from normal bone density. BMC Musculoskelet Disord. 2022;23(1):336. Published 2022 Apr 8. https://doi.org/10.1186/s12891-022-05309-6

Publisher's note